AJNR Am J Neuroradiol 22:1893–1900, November/December 2001

Analysis of Normal-Appearing White Matter in Multiple Sclerosis: Comparison of Diffusion Tensor MR Imaging and Magnetization Transfer Imaging

Alexander C. Guo, Valerie L. Jewells, and James M. Provenzale

BACKGROUND AND PURPOSE: **Our purpose was to compare diffusion tensor MR and magnetization transfer imaging in assessing normal-appearing white matter (WM) regions in multiple sclerosis (MS).**

METHODS: **Diffusion tensor, magnetization transfer, and conventional MR imaging were performed in 12 patients with MS. Fractional anisotropy, apparent diffusion coefficients (ADCs), and magnetization transfer ratios (MTRs) were measured in plaques, normal-appearing periplaque WM (PWM) regions, and normal-appearing WM regions remote from plaques. Mean fractional anisotropy, ADCs, and MTRs were calculated and compared in WM regions.**

RESULTS: **Fractional anisotropy was lower in normal-appearing PWM regions than in remote WM regions ($P < .001$) but higher than in plaques ($P < .001$). MTRs were lower (not significantly, $P = .19$) in normal-appearing PWM regions than in remote regions. MTRs were higher in normal-appearing PWM regions than in plaques ($P < .001$). ADCs were higher in normal-appearing PWM regions than in remote regions ($P = .008$) but lower than in plaques ($P = .001$). Correlation between fractional anisotropy and MTRs of individual lesions was poor ($r = 0.18$) and between fractional anisotropy and ADC, modest ($r = -0.39$).**

CONCLUSION: **In MS, diffusion tensor MR imaging can depict differences between WM regions that are not apparent on conventional MR images. Anisotropy measurements may be more sensitive than those of MTRs in detecting subtle abnormalities in PWM.**

Diffusion tensor MR imaging and magnetization transfer imaging are two promising advances that can provide a means for assessing important physiologic parameters (eg, demyelination, axonal loss) in multiple sclerosis (MS) that cannot be directly assessed at standard MR imaging (1, 2). Magnetization transfer imaging is the more established of the two techniques in MS research, and its findings have been shown to better correlate with disease burden and clinical parameters, such as cognitive impairment, than do those at conventional MR imaging (2). Magnetization transfer imaging also has been useful in extending our understanding of the pathologic evolution of MS lesions (2).

Diffusion tensor MR imaging has received increasing attention because it provides a means for assessing the magnitude and the directionality of water diffusion in tissue. That water diffusion in white matter (WM) is highly directional (ie, anisotropic) is well recognized, because of the orientation of axons and the presence of myelin (3–5). When myelination or axonal integrity is disrupted, a decrease in diffusion anisotropy can be expected (3–5). Decreases in diffusion anisotropy have been shown to occur in association with MS and other disease processes, such as cerebral infarction, amyotrophic lateral sclerosis, progressive multifocal leukoencephalopathy, and Krabbe disease (6–11).

In studies of MS with diffusion tensor MR imaging performed by our group and by other investigators, decreased anisotropy was noted not only within plaques visible on conventional T2-weighted images but also within normal-appearing WM regions (6, 12, 13). We specifically found that anisotropy within normal-appearing periplaque WM (PWM) regions is decreased and intermediate in degree compared with anisotropy within plaques and anisotropy within normal-appearing WM regions remote from plaques (12). These findings are consistent with evidence from magnetization transfer imaging, MR spectroscopy, and histologic studies that suggest extension of disease beyond plaques (14–18). However, in our previous study (12), we used only diffusion-weighted imaging and

Received January 4, 2001; accepted after revision July 16.

From the Department of Radiology, Duke University Medical Center, Durham, NC.

Address reprint requests to Alexander C. Guo, MD, Box 3808, Department of Radiology, Duke University Medical Center, Durham, NC 27710.

did not include magnetization transfer measurements. To our knowledge, no published data that directly correlate diffusion tensor MR imaging with other techniques for the assessment of WM in MS exist (although nontensor diffusion-weighted imaging has been compared with magnetization transfer imaging [19]). Therefore, the purposes of this study were to compare the sensitivities of anisotropy measurements and magnetization transfer ratio (MTR) measurements for the detection of abnormal WM in patients with MS and to confirm that anisotropy values in normal-appearing PWM regions substantially differed from those in plaques and normal-appearing WM regions remote from plaques.

Methods

Patient Population

Twelve patients (four male and eight female patients; mean age, 39 y) with a clinical and radiologic diagnosis of MS underwent diffusion tensor MR imaging and magnetization transfer imaging, as well as conventional MR imaging, during 4 mo (20). Four patients were from a group of 26 patients included in our previous study (12) of MS with diffusion tensor MR imaging. All 12 patients had the relapsing-remitting form of disease. The duration of clinically evident disease was 2–11 y at the time of imaging. Two patients had relative worsening of symptoms at the time of imaging. Quantitative disability scores, such as the Expanded Disability Status Scale scores, were not obtained.

MR Data Acquisition

Imaging was performed by using 1.5-T clinical MR imagers (Signa; GE Medical Systems, Milwaukee, WI), with a standard head coil and without cardiac gating. Diffusion tensor MR imaging was performed by using single-shot spin-echo echo-planar imaging with 12,000/107/2200/1 (TR/TE/TI/excitations) and diffusion gradient encoding in six directions with $b = 1000$ s/mm^2 or no diffusion gradient ($b = 0$). Images were obtained through the entire brain, with seven diffusion-weighted images obtained for each 5-mm-thick image section (section gap, 2.5 mm). The matrix size was 128×64 pixels for a field of view of 40×20 cm. An acquisition time of approximately 2 min was required for this diffusion tensor MR imaging sequence. Diffusion tensor MR imaging was performed as a part of our routine protocol for patients with MS, as approved by our institutional review board.

Conventional MR images also were obtained and included axial proton density–weighted and T2-weighted images. The sequence parameters were 2800/30/2 (TR/TE/excitations, first echo) and 2800/100/2 (second echo); field of view, 22×22 cm; matrix size, 256 (frequency direction) $\times$ 192 (phase direction); section thickness, 5 mm; and section gap, 2.5 mm.

Magnetization transfer imaging was performed by adding an off-resonance sinc-shaped saturation pulse at an offset frequency of 1000 Hz (below the resonance frequency of free water) to a conventional spin-echo proton density–weighted sequence (same proton density–weighted sequence as before). Additional parameters for the off-resonance saturation pulse were pulse width, 16 ms; amplitude, $0.438 \times$ the amplitude of the 180° pulse; and flip angle, 1100°. A spin-echo sequence was chosen rather than a gradient-echo sequence because of its better signal-to-noise ratio. A high signal-to-noise ratio was desirable for our study because of the need to distinguish relatively small differences in magnetization transfer effects that were expected between normal-appearing PWM regions and normal-appearing WM regions remote from plaques. The spin-echo technique was used with the realization that magnetization transfer image data obtained with this technique may not have been directly comparable with data from studies with the gradient-echo technique.

MR Data Analysis

The diffusion imaging data were processed by using the GE software program Functool as well as proprietary software on an independent workstation (Advantage Windows; GE Medical Systems). The six independent elements of the diffusion tensor and its eigenvalues were calculated with the method that Basser (3) described. Fractional anisotropy was then calculated according to the following equation: $FA = (3/2)^{1/2} [(E_1 - d)^2 + (E_2 - d)^2 + (E_3 - d)^2]^{1/2}/(E_1^2 + E_2^2 + E_3^2)^{1/2}$, where FA = fractional anisotropy, E_i is one of the three eigenvalues, and d is $(E_1 + E_2 + E_3)/3$ (3, 10). Diffusivity can be thought of as the sum of an isotropic fraction and an anisotropic fraction. Fractional anisotropy represents the anisotropic portion of diffusivity. Fractional anisotropy was chosen as the index of anisotropy because it is rotationally invariant and provides a relatively high contrast-to-noise ratio compared with that of other indices, such as volume ratio and relative anisotropy (3, 4, 10). Values for fractional anisotropy range from 0 to 1, where 0 represents isotropic diffusion, and 1 represents highly anisotropic diffusion. Fractional anisotropy is a unitless ratio of diffusion coefficients. All calculations noted here were performed automatically on a voxel-by-voxel basis by using the software, and the fractional anisotropy values were displayed as an anisotropy map.

Apparent diffusion coefficient (ADC) maps also were generated from diffusion tensor data by using Functool software and by applying the following equation: $ADC = (E_1 + E_2 + E_3)/3$, where E_i is one of the three eigenvalues (ie, ADC is the average of the three eigenvalues). ADC measurements were obtained to provide another means for comparing our diffusion imaging data with data from other investigators, because in published studies ADC was used far more often than was anisotropy to assess MS lesions.

A comparison of magnetization transfer histograms, with an attempt to generate anisotropy histograms, was initially investigated, because histograms have the advantage of providing an estimate of whole-brain lesion load, being less susceptible to observer bias, and having a comparable measure in magnetization transfer histograms. Both magnetization transfer and ADC histograms for the evaluation of MS have also been reported in the recent literature (17–19, 21–23). However, anisotropy maps generated on our system had a poor signal-to-noise ratio because of the limited imaging time. These maps produced broad histograms that were not useful for distinguishing subtle abnormalities in WM anisotropy values. Therefore, we proceeded to measure fractional anisotropy and MTR by using regions of interest (ROIs), which also provided the ability to selectively measure small regions of WM.

A single neuroradiologist who was blinded to the patient's identity and clinical status initially placed the ROIs on the T2-weighted images, which were drawn semiautomatically by using the Functool software. Uniform ovoid ROIs were drawn in every plaque that was large enough to accommodate a 78-mm^2 ROI without apparent volume averaging of surrounding brain (minimum plaque size of approximately 100 mm^2) (Fig 1A). A total of 36 plaques were assessed in 12 patients.

The fractional anisotropy and ADC maps were superimposed on the conventional T2-weighted images by using the Functool software, which interpolates the images if different image sizes are encountered. The coregistration of the images can then be refined manually by means of translation and rotation with proprietary software. The software then automatically transferred the ROIs to the coregistered fractional anisotropy and ADC maps (Fig 1B and C), and average fractional anisotropy and ADC values within the ROIs were recorded.

The ROI were all 78 ± 20 mm^2, which is equivalent to 6–10 pixels.

A second neuroradiologist who was blinded to the anisotropy data, patient's identity, and clinical status assessed the MTRs. ROIs recorded on T2-weighted images were used to generate matching ROIs on proton density–weighted images obtained before and after application of a magnetization transfer saturation pulse (Fig 1D and E). MTRs were calculated for each ROI by using the following equation: $MTR = M_0 - M_S/M_0$, where M_S is the average signal intensity within a given ROI measured after application of an off-resonance saturation pulse, and M_0 is the average signal intensity within the same ROI before application of the saturation pulse.

Uniform ROIs also were drawn in normal-appearing PWM regions, which were defined as the WM closest to and surrounding the plaque that was not abnormal in signal intensity on coregistered T2-weighted images. These ROIs were the same size as those drawn in plaques but were more elongated to allow measurement of WM immediately adjacent to plaques. ROIs in normal-appearing PWM regions were placed at 90° angles to form a box surrounding the plaque (Fig 1F) . If a normal-appearing PWM ROI overlapped CSF or gray matter, it was discarded; 16 ROIs were excluded on that basis. Fractional anisotropy values for the ROIs (three or four in number) surrounding each plaque were averaged and then recorded as a single number. The same procedure was performed for ADC and MTR values. A total of 130 normal-appearing PWM regions were assessed in 12 patients.

Uniform ROIs also were drawn in normal-appearing WM regions remote from plaques. One ROI was drawn in normal-appearing WM regions remote from plaques for each plaque. The normal-appearing WM region remote from plaques paired with each plaque was usually at the same location as the plaque but in the contralateral hemisphere (Fig 1). However, when abnormal signal intensity was seen within the structure of the matching normal-appearing WM regions remote from plaques, a similar WM structure in the contralateral hemisphere was measured. It was necessary to match the normal-appearing WM regions remote from plaques as closely to the plaque as possible because marked intrinsic variations in anisotropy exist between different WM structures (24). After ROIs were placed, the values for fractional anisotropy, ADC, and MTR values were recorded. A total of 36 normal-appearing WM regions remote from plaques were assessed in 12 patients.

Fractional anisotropy, MTR, and ADC values were compared between the following pairs of structures by using a paired Student *t* test: plaques and normal-appearing PWM regions, normal-appearing PWM regions and normal-appearing WM regions remote from plaques, and plaques and normal-appearing WM regions remote from plaques. A paired Student *t* test was used because of the aforementioned substantial intrinsic variations in anisotropy between WM structures, which required pairing of each plaque with its own normal-appearing PWM regions and closely matched normal-appearing WM regions remote from plaques. A P value $< .05$ was considered significant in all cases. Fractional anisotropy values were then correlated with MTR values and ADC values by calculating the Pearson correlation coefficient.

Results

Regional Fractional Anisotropy Values

Fractional anisotropy (plaques) was 0.302 ± 0.095, fractional anisotropy (normal-appearing PWM regions) was 0.359 ± 0.056, and fractional anisotropy (normal-appearing WM regions remote from plaques) was 0.462 ± 0.111. The lowest fractional anisotropy was measured in plaques, with the next lowest in normal-appearing PWM regions and the next lowest in normal-appearing WM regions remote from plaques. Statistically significant differences in fractional anisotropy between plaques and normal-appearing PWM regions ($P < .001$), between plaques and normal-appearing WM regions remote from plaques ($P < .001$), and between normal-appearing PWM regions and normal-appearing WM regions remote from plaques ($P < .001$) were found.

Regional MTR Values

MTR (plaque) was 0.529 ± 0.046, MTR (normal-appearing PWM regions) was 0.554 ± 0.038, and MTR (normal-appearing WM regions remote from plaques) was 0.561 ± 0.033. The lowest MTR was measured in plaques, with the next lowest in normal-appearing PWM regions and the next lowest in normal-appearing WM regions remote from plaques. Statistically significant differences in MTR between plaques and normal-appearing PWM regions ($P < .001$) and between plaques and normal-appearing WM regions remote from plaques ($P < .001$) were noted. Although MTR in normal-appearing PWM regions was slightly lower than in normal-appearing WM regions remote from plaques, the difference was not statistically significant ($P = .19$).

Regional ADC Values

ADC (plaque) was $(0.901 \pm 0.095) \times 10^{-3}$ mm^2/s, ADC (normal-appearing PWM regions) was $(0.793 \pm 0.078) \times 10^{-3}$ mm^2/s, ADC (normal-appearing WM regions remote from plaques) was $(0.764 \pm 0.038) \times 10^{-3}$ mm^2/s. The highest ADC values were measured in plaques, with the next highest in normal-appearing PWM regions and the next highest in normal-appearing WM regions remote from plaques. Statistically significant differences between plaques and normal-appearing PWM regions ($P < .001$), between plaques and normal-appearing WM regions remote from plaques ($P < .001$), and between normal-appearing PWM regions and normal-appearing WM regions remote from plaques ($P = .008$) were found.

Correlation of Fractional Anisotropy with MTR and with ADC

When values of fractional anisotropy and MTR were correlated for each lesion, the correlation was weak ($r = 0.18$). However, when mean values of fractional anisotropy and MTR for each WM region (plaque, normal-appearing PWM regions, and normal-appearing WM regions remote from plaques) were correlated, a strong correlation was seen ($r = 0.89$). The negative correlation between fractional anisotropy and ADC values of individual plaques ($r = -0.39$) was stronger than the correlation between fractional anisotropy and MTRs, although it was still modest. However, when mean

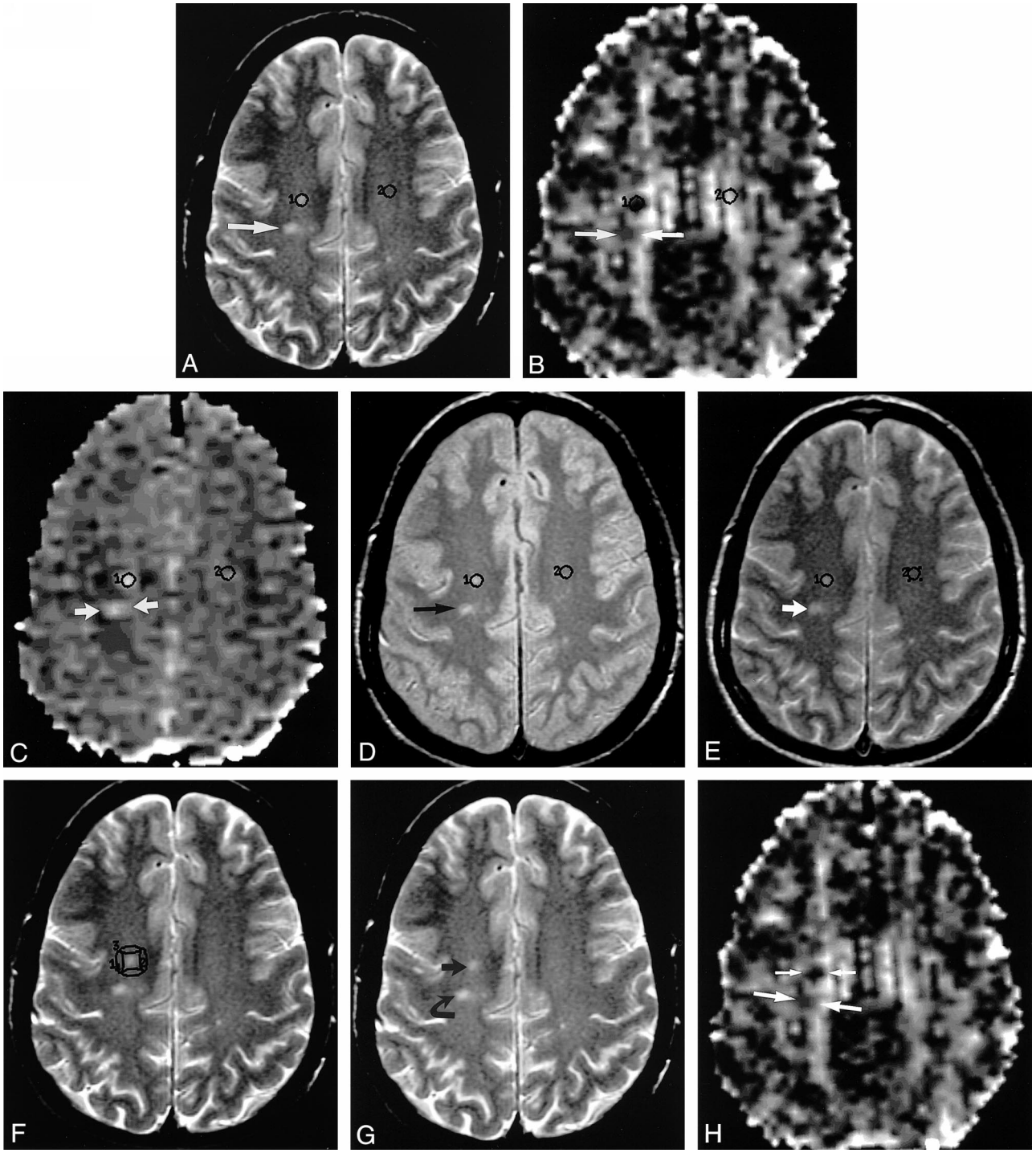

FIG 1. Axial MR images in a 42-year-old patient with MS.

A, T2-weighted image (2800/100/2) obtained at the level just above the roof of lateral ventricles shows some of the ROIs used. ROI labeled *1* overlies a plaque in the right centrum semiovale. ROI labeled *2* overlies a matching WM region in the left centrum semiovale. *Arrow* indicates a second plaque located more posteriorly.

B, Diffusion tensor MR image–derived anisotropy map obtained by using single-shot spin-echo echo-planar imaging (12,000/107/2200/1, b = 1000 s/mm^2 in six directions, and b = 0) at the same anatomic level as in *A* shows placement of ROIs on the same structures as in *A.* The second plaque in *A* is bracketed by the *arrows* on this image.

C, Diffusion tensor MR image–derived ADC map obtained by using single-shot spin-echo echo-planar imaging with (12,000/107/2200/1, b = 1000 s/mm^2 in six directions, and b = 0) at the same anatomic level as in *A* shows placement of ROIs on the same structures as in *A.* The second plaque in *A* is bracketed by the *arrows* on this image.

D, Proton density–weighted image (2800/30/2) obtained at the same anatomic level as in *A,* before the application of magnetization transfer saturation pulse, shows an ROI labeled *1* overlying a plaque in the right centrum semiovale and an ROI labeled *2* overlying a matching WM region in the left centrum semiovale (normal-appearing WM regions remote from plaques). *Arrow* indicates a second plaque located more posteriorly.

E, Proton density–weighted image (2800/30/2) obtained at the same anatomic level as in *A,* after the application of magnetization

values of fractional anisotropy and ADC for each WM region were correlated, the negative correlation was much stronger ($r = -0.93$). The correlation between ADC and MTR values of individual lesions was weak ($r = 0.05$), but once again, the correlation of mean ADC and MTR value for each WM region was strong ($r = -0.99$).

Discussion

Comparison of Fractional Anisotropy with MTRs

For individual lesions, the correlation between fractional anisotropy and MTR was modest ($r = 0.18$). In addition, although a significant difference in MTRs was measured between plaques and normal-appearing WM regions remote from plaques, the amount of MTR reduction was proportionally less than the amount of fractional anisotropy reduction. The relatively poor correlation between fractional anisotropy and MTRs in individual plaques and the greater differences measured by using fractional anisotropy may reflect the different influences of MS pathophysiologic anisotropy and MTR values. Demyelination and disruption of axonal integrity are two pathologic hallmarks of MS plaques, but inflammation and edema also are important components, especially in acute plaques (25). Anisotropy measurements are sensitive to demyelination and axonal degeneration and also the presence of edema and inflammatory infiltrates (5–10). In contrast, MTR measurements are less sensitive to the latter two factors. Studies of demyelinating diseases in human volunteers and animal models have shown that demyelination and axonal loss are major contributors to decreases in MTR, whereas inflammation and edema provide relatively minor contributions to MTR reduction (26). Postmortem studies have also shown that a strong positive correlation between axonal density and MTR exists (27). Therefore, it is possible that anisotropy measurements are more sensitive in depicting abnormal WM in general, whereas MTR measurements are more specific in showing areas of substantial demyelination and axonal degeneration.

The finding of decreased anisotropy in normal-appearing PWM regions compared with that in normal-appearing WM regions remote from plaques confirms the results of our previous investigation and suggests extension of the disease process in MS beyond the plaque boundary. Multiple groups of investigators (14, 28–30) have found significant decreases in the *N*-acetylaspartate and *N*-acetylaspartate–creatine ratio (which are markers for neuronal or axonal damage) in normal-appearing WM in patients with MS. One group (14) specifically noted a decreased *N*-acetylaspartate–creatine ratio in normal-appearing WM adjacent to plaques, which occurred to a greater extent in these areas than in WM regions remote from plaques. Histopathologic studies also have revealed axonal loss and axonal transection in normal-appearing WM (15, 31, 32); one recent report noted axonal damage in periplaque regions surrounding acutely demyelinating plaques (15).

MTR measurements in normal-appearing PWM regions also were decreased compared with those of normal-appearing WM regions remote from plaques, although the difference was not statistically significant ($P = .19$). Multiple investigators (16–18, 23, 33–36) have noted evidence of abnormal MTR in normal-appearing WM. Investigators (16) who specifically measured MTR in normal-appearing WM regions adjacent to isolated plaques have observed that MTR gradually increases (and approaches values in normal-appearing WM regions remote from plaques) as one moves away from plaques. Bagley et al (33), using MTR contour plots, also found a gradual increase in MTR values as one moved away from the plaque. These results not only support our findings but also suggest a gradient of WM abnormality extending centrifugally from the plaque.

The observations of decreased diffusion anisotropy (and to a lesser extent, MTR) in normal-appearing PWM regions are consistent with the known natural history of MS plaques. Studies in which imaging and histopathologic data were correlated have revealed that MS plaques begin as a perivenular focus of inflammation, which expands in a centrifugal manner (25). As acute MS plaques become inactive and regress, they often diminish in size on T2-weighted images, and both myelin breakdown products and transected axons can be found in the periphery of active and reactivated chronic plaques (14, 15, 25, 37).

Our findings also can be partially explained with the results of recent serial diffusion-weighted MR imaging studies. These studies revealed a subtle but significant increase in ADC within prelesional WM regions where plaques subsequently appear (38, 39). Similarly, a recent magnetization transfer imaging study (34) also has revealed decreased MTR

←

transfer saturation pulse with an offset frequency of 1000 Hz, shows an ROI labeled *1* overlying a plaque in the right centrum semiovale and an ROI labeled *2* overlying a matching WM region in the left centrum semiovale. *Arrow* indicates a second plaque located more posteriorly.

F, Same T2-weighted image as in *A* shows additional ROIs labeled *1, 2, 3,* and *4* overlying normal-appearing PWM regions in the right centrum semiovale.

G, Same T2-weighted image as in *A,* without ROIs, shows plaques *1* (*straight arrow*) and *2* (*curved arrow*) in *A.*

H, Same diffusion tensor MR image–derived anisotropy map as in *B,* obtained at the same anatomic level as in *G,* shows the areas of signal intensity abnormality in the right centrum semiovale corresponding to the first (*short arrows*) and second (*long arrows*) plaques in *G.*

in prelesional WM regions. The subset of normal-appearing PWM regions associated with expanding acute plaques in our series may be pathophysiologically similar to the prelesional WM regions in these reports. However, this hypothesis needs further validation with longitudinal studies.

Our results also revealed significantly lower fractional anisotropy in plaques, compared with those of either normal-appearing PWM regions or normal-appearing WM regions remote from plaques, as we found in our previous study. A greater anisotropy decrease in plaques relative to normal-appearing WM, which other investigators have also reported, is an expected finding. As noted above, demyelination and disruption of axonal integrity are two pathologic hallmarks of MS plaques, but inflammation and edema also play important roles in MS (25). All these pathologic processes have been shown to be associated with decreased diffusion anisotropy, and they are likely to be more extensive within plaques than in normal-appearing WM (5–11, 28–32). MTR also was found to be significantly lower in plaques than in normal-appearing PWM regions or normal-appearing WM regions remote from plaques, as one would expect.

Comparison of Anisotropy Measurements with Previous Findings

Relatively few groups have assessed WM anisotropy in patients with MS. An echo-planar imaging technique was also used in the four studies (with which we compared ours) , and fractional anisotropy was the anisotropy index of choice in all studies (6, 7, 12, 13). We assessed normal-appearing PWM regions in our previous study, but the other authors did not. The mean fractional anisotropy of 0.359 measured in normal-appearing PWM regions in this study was similar to the mean fractional anisotropy measured in our previous study, 0.383 (12). In normal-appearing WM regions remote from plaques, the mean fractional anisotropy of 0.462 measured in this study also was similar to the mean fractional anisotropy of 0.493 measured in our previous study (12). It also is within the range of 0.404 to 0.56 that other authors observed (6, 7, 13). The mean fractional anisotropy measured in plaques in this study was 0.302, which is similar to the mean fractional anisotropy of 0.280 in our previous study (12). This value also lies within the range of 0.23 to 0.43 that Bammer et al (13) reported for nonacute (nonhomogeneously enhancing) plaques, and it is similar to the mean fractional anisotropy of 0.278 that Tievsky et al (7) reported for subacute plaques and of 0.289 for chronic plaques. Compared with the mean fractional anisotropy of 0.50 that Werring et al (6) reported in a small series, our mean fractional anisotropy for plaques was substantially lower, possibly because of differences in plaque population or imaging technique.

Correlation of ADC with Fractional Anisotropy, MTR, and Previous Findings

ADC values also were measured in this study to provide another means for comparison with fractional anisotropy and MTR value and with those of other studies. ADC was chosen because multiple previous studies (6, 7, 19, 35, 40–43) have shown that ADC is increased in plaques and normal-appearing WM regions remote from plaques. A modest inverse correlation between ADC values and fractional anisotropy values of individual lesions ($r = -0.39$) was seen and was stronger than the correlation between fractional anisotropy and MTR ($r = 0.18$). The inverse correlation between decreased fractional anisotropy and increased ADC suggests that the pathologic processes in MS result in both an increase in overall water diffusibility and a decrease in diffusion anisotropy. In several recent studies, ADC values in plaques were observed to be 0.92×10^{-3} to 1.59×10^{-3} mm^2/s (6, 7, 19, 35, 40–43). Our measurement of 0.901×10^{-3} mm^2/s for plaques is consistent with these values. In the same studies, ADC values in normal-appearing WM regions remote from plaques were observed to be 0.69×10^{-3} to 0.88×10^{-3} mm^2/s. Our measurement for ADC in normal-appearing WM regions remote from plaques of 0.764×10^{-3} mm^2/s also occurs within this range. Previous investigators (6, 7, 19, 35, 40–43) have suggested that lesions of different ages, different T1-weighted characteristics, and different enhancement patterns have different diffusion characteristics. Unfortunately, the number of enhancing or hypointense plaques on T1-weighted images in our study group was insufficient to provide meaningful comparisons.

One previous group (19) compared ADCs and MTRs in lesions, normal-appearing WM regions remote from plaques, and controls. Although they analyzed several normal-appearing WM regions remote from plaques on the basis of anatomy, the investigators did not analyze normal-appearing PWM regions separately. These investigators found that ADCs were significantly higher and MTRs were significantly lower in lesions compared with normal-appearing WM regions remote from plaques, as we did. They also found a strong inverse correlation between ADC and MTR in lesions ($r = -0.7$). Although we did not find a strong correlation between ADC and MTR in individual lesions ($r = 0.05$), we did find a strong inverse correlation between mean ADC and mean MTR of various WM regions ($r = -0.99$).

One limitation of this study is the lack of healthy control subjects. Without a control group, we cannot be certain that fractional anisotropy measurements in any of the WM regions in our patients were actually abnormal. However, our previous study, which has a control group, revealed similar fractional anisotropy in plaque, normal-appearing PWM regions, and normal-appearing WM regions remote from plaques, which were all decreased

compared with that of control subjects. Also, this was a preliminary study, with a relatively small number of patients, in which we were not able to correlate our findings with quantitative clinical assessment of patients (eg, the Expanded Disability Status Scale score) or to incorporate longitudinal data. From a technical prospective, the spatial resolution of diffusion tensor MR imaging was relatively poor, and the anisotropy maps had a certain amount of spatial distortion (as with all image data derived from an echo-planar imaging technique), which limited precise registration of the anisotropy and ADC maps with the conventional MR images. This problem was the reason for excluding lesions smaller than approximately 100 mm^2 and for using ROIs larger than 58 mm^2 (6 pixels) to minimize errors due to volume averaging. The use of a 2.5-mm spacing between sections would have been suboptimal if we included smaller lesions in our analysis, but it did not impose additional limitations, because we excluded lesions smaller than approximately 1 cm in diameter (100 mm^2). This exclusion introduced a selection bias toward larger MS plaques.

Conclusion

Both anisotropy and MTR measurements showed differences between normal-appearing PWM regions and normal-appearing WM regions remote from plaques in patients with MS that were not apparent on conventional T2-weighted images. However, the difference was significant only with anisotropy measurements; this finding suggested that diffusion tensor MR imaging may be more sensitive than magnetization transfer imaging in depicting subtle WM disease in patients with MS. Therefore, diffusion tensor MR imaging provides important additional information that may be useful in trials of novel therapeutic agents and likely represents a distinct advance compared with conventional T2-weighted imaging. Future studies correlating global quantitative measures of diffusion anisotropy with clinical status are warranted.

References

1. Miller DH, Grossman RI, Reingold SC, McFarland HF. **The role of magnetic resonance techniques in understanding and managing multiple sclerosis.** *Brain* 1998;121:3–24
2. Grossman RI. **Application of magnetization transfer imaging to multiple sclerosis.** *Neurology* 1999;53:S8–S11
3. Basser P. **Inferring microstructural features and the physiological state of tissues from diffusion-weighted images.** *NMR Biomed* 1995;8:333–344
4. Pierpaoli C, Jezzard P, Basser PJ, Barnett A, Di Chiro G. **Diffusion tensor MR imaging of the human brain.** *Radiology* 1996; 201:637–648
5. Beaulieu C, Allen PS. **Determinants of anisotropic water diffusion in nerves.** *Magn Reson Med* 1994;31:394–400
6. Werring DJ, Clark CA, Barker GJ, Thompson AJ, Miller DH. **Diffusion tensor imaging of lesions and normal-appearing white matter in multiple sclerosis.** *Neurology* 1999;52: 1626–1632
7. Tievsky AL, Ptak T, Farkas J. **Investigation of apparent diffusion coefficient and diffusion tensor anisotropy in acute and chronic multiple sclerosis lesions.** *AJNR Am J Neuroradiol* 1999; 20:1491–1499
8. Hajnal JV, Doran M, Hall AS, et al. **MR imaging of anisotropically restricted diffusion of water in the central nervous system: technical, anatomic, and pathologic considerations.** *J Comput Assist Tomogr* 1991;15:1–18
9. Ulug AM, Moore DF, Bojko AS, Zimmerman RD. **Clinical use of diffusion-tensor imaging for diseases causing neuronal and axonal damage.** *AJNR Am J Neuroradiol* 1999;20:1044–1048
10. Sorensen AG, Wu O, Copen WA, et al. **Human acute cerebral ischemia: detection of changes in water diffusion anisotropy by using MR imaging.** *Radiology* 1999;212:785–792
11. Guo AC, Petrella JR, Kurtzberg J, Provenzale JM. **Evaluation of white matter anisotropy in Krabbe disease using diffusion tensor MR imaging: initial experience.** *Radiology* 2001;218: 809–815
12. Guo AC, MacFall J, Provenzale JM. **Diffusion tensor MR imaging of multiple sclerosis: evaluation of normal-appearing white matter.** *Radiology* (in press)
13. Bammer R, Augustin M, Strasser-Fuchs S, et al. **Magnetic resonance diffusion tensor imaging for characterizing diffuse and focal white matter abnormalities in multiple sclerosis.** *Magn Reson Med* 2000;44:583–591
14. Arnold DL, Matthews PM, Francis GS, O'Connor J, Antel JP. **Proton magnetic resonance spectroscopic imaging for metabolic characterization of demyelinating plaques.** *Ann Neurol* 1992;31:235–241
15. Kornek B, Storch MK, Weissert R, et al. **Multiple sclerosis and chronic autoimmune encephalomyelitis: a comparative quantitative study of axonal injury in active, inactive, and remyelinated lesions.** *Am J Pathol* 2000;157:267–276
16. Filippi M, Campi A, Dousset V, et al. **A magnetization transfer imaging study of normal-appearing white matter in multiple sclerosis.** *Neurology* 1995;45:478–482
17. Catalaa I, Grossman RI, Kolson DL, et al. **Multiple sclerosis: magnetization transfer histogram analysis of segmented normal-appearing white matter.** *Radiology* 2000;216:351–355
18. Tortorella C, Viti B, Bozzali M, et al. **A magnetization transfer histogram study of normal-appearing brain tissue in MS.** *Neurology* 2000;54:186–193
19. Cercignani M, Iannucci G, Rocca MA, Comi G, Horsfield MA, Filippi M. **Pathologic damage in MS assessed by diffusion-weighted and magnetization transfer MRI.** *Neurology* 2000;54: 1139–1144
20. Poser CM, Paty DW, Scheinberg L, et al. **New diagnostic criteria for multiple sclerosis: guidelines for research protocols.** *Ann Neurol* 1983;13:227–231
21. Nusbaum AO, Tang CY, Wei T, Buchsbaum MS, Atlas SW. **Whole-brain diffusion MR histograms differ between MS subtypes.** *Neurology* 2000;54:1421–1427
22. Van Buchem M, McGowan JC, Grossman RI. **Magnetization transfer histogram methodology: its clinical and neuropsychological correlates.** *Neurology* 1999;53:S23–S28
23. Filippi M, Inglese M, Rovaris M, et al. **Magnetization transfer imaging to monitor the evolution of MS: a 1-year follow-up study.** *Neurology* 2000;55:940–946
24. Shimony JS, McKinstry RC, Akbudak E, et al. **Quantitative diffusion-tensor anisotropy brain MR imaging: normative human data and anatomic analysis.** *Radiology* 1999;212:770–784
25. McDonald WI, Miller DH, Barnes D. **The pathological evolution of multiple sclerosis.** *Neuropathol Appl Neurobiol* 1992;18: 319–334
26. Brochet B, Dousset V. **Pathological correlates of magnetization transfer imaging abnormalities in animal models and humans with multiple sclerosis.** *Neurology* 1999;53:S12–S17
27. Van Waesberghe JH, Kamphorst W, De Groot CJ, et al. **Axonal loss in multiple sclerosis lesions: magnetic resonance imaging insights into substrates of disability.** *Ann Neurol* 1999;46: 747–754
28. Fu L, Matthews PM, De Stefano N, et al. **Imaging axonal damage of normal appearing white matter in multiple sclerosis.** *Brain* 1998;121:103–113
29. Davie CA, Barker GJ, Thompson AJ, Tofts PS, McDonald WI, Miller DH. **^{1}H magnetic resonance spectroscopy of chronic white matter lesions and normal appearing white matter in multiple sclerosis.** *J Neurol Neurosurg Psychiatry* 1997;63: 736–742
30. Leary SM, Davie CA, Parker GJ, et al. **^{1}H magnetic resonance spectroscopy of normal appearing white matter in primary progressive multiple sclerosis.** *J Neurol* 1999;246:1023–1026

31. Allen IJ, McKeown SR. **A histological, histochemical and biochemical study of the macroscopically normal white matter in multiple sclerosis.** *J Neurol Sci* 1979;41:81–91
32. Evangelou N, Esiri MM, Smith S, Palace J, Matthews PM. **Quantitative pathological evidence for axonal loss in normal appearing white matter in multiple sclerosis.** *Ann Neurol* 2000; 47:391–395
33. Bagley LJ, Grossman RI, Galetta SL, Sinson GP, Kotapka M, McGowen JC. **Characterization of white matter lesions in multiple sclerosis and traumatic brain injury as revealed by magnetization transfer contour plots.** *AJNR Am J Neuroradiol* 1999; 20:977–981
34. Pike GB, De Stefano N, Narayanan S, et al. **Multiple sclerosis: magnetization transfer MR imaging of white matter before lesion appearance on T2-weighted images.** *Radiology* 2000;215: 824–830
35. Filippi M, Iannucci G, Cercignani M, Assunta Rocca M, Pratesi A, Comi G. **A quantitative study of water diffusion in multiple sclerosis lesions and normal-appearing white matter using echo-planar imaging.** *Arch Neurol* 2000;57:1017–1021
36. Loevner LA, Grossman RI, Cohen JA, Lexa FJ, Kessler D, Kolson DL. **Microscopic disease in normal-appearing white matter on conventional MR images in patients with multiple sclerosis: assessment with magnetization transfer measurements.** *Radiology* 1995;196:511–515
37. Waxman SG. **Demyelinating diseases: new pathological insights, new therapeutic targets.** *N Engl J Med* 1998;338: 323–325
38. Rocca MA, Cercignani M, Iannucci G, Comi G, Filippi M. **Weekly diffusion-weighted imaging of normal-appearing white matter in MS.** *Neurology* 2000;55:882–884
39. Werring DJ, Brassat D, Droogan AG, et al. **The pathogenesis of lesions and normal-appearing white matter changes in multiple sclerosis: a serial diffusion MRI study.** *Brain* 2000;123: 1667–1676
40. Castriota-Scanderbeg A, Tomaiuolo F, Sabatini U, Nocentini U, Grasso MG, Caltagirone C. **Demyelinating plaques in relapsing-remitting and secondary-progressive multiple sclerosis: assessment with diffusion MR imaging.** *AJNR Am J Neuroradiol* 2000; 21:862–868
41. Tsuchiya K, Hachiya J, Maehara T. **Diffusion-weighted MR imaging in multiple sclerosis: comparison with contrast-enhanced study.** *Eur J Radiol* 1999;31:165–169
42. Roychowdhury S, Maldjian JA, Grossman RI. **Multiple sclerosis: comparison of trace apparent diffusion coefficients with MR enhancement pattern of lesions.** *AJNR Am J Neuroradiol* 2000; 21:869–874
43. Horsfield MA, Lai M, Webb SL, et al. **Apparent diffusion coefficients in benign and secondary progressive multiple sclerosis by nuclear magnetic resonance.** *Magn Reson Med* 1996; 36:393–400